ARTICLES

Cross sections and analyzing powers for the $(\vec{p},n)$ reaction on ^{3}He and ^{4}He at 200 MeV

M. Palarczyk,* C. M. Riedel,† D. Dehnhard, M. A. Espy,† M. A. Franey, and J. L. Langenbrunner†
School of Physics and Astronomy, University of Minnesota, Minneapolis, Minnesota 55455

L. C. Bland and D. S. Carman‡
Indiana University Cyclotron Facility, Bloomington, Indiana 47408

B. Brinkmöller§
Physikalisches Institut der Universität Karlsruhe, Karlsruhe, Germany

R. Madey, Y. Wang,‖ and J. W. Watson
Department of Physics, Kent State University, Kent, Ohio 44242

N. S. Chant
Department of Physics, University of Maryland, College Park, Maryland 20742
(Received 31 December 1997)

Double-differential cross sections and analyzing powers A_y for the $(\vec{p},n)$ reactions on ^{3}He and ^{4}He were measured at 200 MeV between $\theta_{lab}=0°$ and 44°. The neutron spectra from ^{3}He$(\vec{p},n)$ are dominated by the quasifree scattering peak and show no evidence for resonances in the three-proton system. The spectra from ^{4}He$(\vec{p},n)$ exhibit strong resonance behavior in the p^3He system at low relative p^3He energies owing to the excitation of known $L=1$ resonances in ^{4}Li, but there is no distinct quasifree peak in the measured spectra. The experimental A_y for ^{3}He$(\vec{p},n)$, averaged over the experimental range of neutron energies, are similar to those for free nucleon-nucleon (NN) scattering, whereas for ^{4}He$(\vec{p},n)$ the A_y are generally larger than the free values. The cross sections at far forward angles for both ^{3}He and ^{4}He appear to be suppressed relative to the free NN cross sections by Pauli blocking. At most angles, the shapes of the cross section spectra from both ^{3}He and ^{4}He are reproduced by distorted-wave impulse approximation (DWIA) calculations using a quasifree scattering model. Specifically for ^{4}He$(\vec{p},n)$, the model requires the use of an optical potential which has a strong $L=1$ potential resonance corresponding to the low-lying $L=1$ states in ^{4}Li. [S0556-2813(98)00908-X]

PACS number(s): 25.10.+s, 25.40.Kv, 24.70.+s, 27.10.+h

I. INTRODUCTION

Systematic studies of (p,n) charge exchange reactions at intermediate energies have been performed on a wide range of nuclei from ^{2}H to ^{238}U. (See the recent review in Ref. [1].) Quasifree (QF) charge exchange experiments have attracted particular attention because they determine both the longitudinal and transverse parts of the QF isovector spin response of nuclei, whereas (e,e') QF scattering exclusively probes the transverse part. Generally, significant differences, containing important information on the nature of the nucleon-nucleon (NN) force in nuclei, are found between (p,n) data and model predictions: for example, the position of the QF peak centroid is observed [1–3] at higher excitation energy than expected and the theoretical spectral shapes require a momentum-transfer (q) dependent renormalization in order to fit the data; however, QF analyzing powers are often in good agreement with the free NN scattering values. See the results for p-shell nuclei at incident energies $T_p=186$ MeV [2] and for ^{12}C and ^{208}Pb at $T_p=495$ MeV [3]. But a significant suppression of A_y has been observed for ^{12}C(p,n) at 795 MeV [3]. None of the discrepancies are understood fully, although a simple explanation for the shift of the centroid has been suggested [4].

Discrepancies between data and first-order model predictions may arise, for example, from multiple-scattering effects or from modifications of the elementary NN force in the nuclear medium. Multiple scattering is expected to be much less important for very light nuclei such as ^{3}He and ^{4}He than for medium and heavy nuclei. Use of ^{3}He and ^{4}He targets for QF scattering studies is particularly attractive because theory provides reliable wave functions for the three- and

*Present address: Ohio University, Athens, OH 45701. Permanent address: Henryk Niewodniczański Institute of Nuclear Physics, 31-342 Kraków, Poland.
†Present address: Los Alamos National Laboratory, Los Alamos, NM 87545.
‡Present address: Carnegie Mellon University, Pittsburgh, PA 15213.
§Present address: S.A.P.-A.G., Karlsruhe, Germany.
‖Present address: St. Francis Hospital, Topeka, KS 66606.

four-nucleon systems. Thus modifications of the *NN* force in nuclei can be studied without uncertainties in the nuclear structure and without large complications from multiple scattering.

According to Faddeev calculations [5–8] of the ground state (g.s.) of ^{3}He, its spin results primarily from the unpaired neutron, and its spatial wave function is dominated by the space-symmetric S state ($\approx 90\%$). There are several D-state components resulting from the tensor *NN* force, totaling about 10% and other small components of the order of 1%, including S'-state components of ''mixed symmetry.'' For the ^{4}He g.s., Green's function Monte Carlo (GFMC) methods [9] predict a D-state admixture larger than for ^{3}He (12%–17% for slightly different models), but the space-symmetric S state is also the dominating configuration ($\approx 82\%$). Thus, for both ^{3}He and ^{4}He, the target wave functions are dominated by the space-symmetric S state in which pairs of identical target nucleons are in spin-singlet states. As a consequence, (p,n) transitions with no angular momentum transfer ($\Delta L = 0$) are expected to be strongly suppressed for both ^{3}He and ^{4}He by Pauli blocking; that is, the proton produced by charge exchange on a target neutron is prohibited from occupying the same space and spin state as either of the two spectator protons. Pauli blocking will be discussed further in Secs. III and IV.

Recent experiments that measured the spin-transfer variables [10] are currently being analyzed. Several measurements of the spin-correlation parameters of the exclusive $^3\vec{\mathrm{He}}(\vec{p},pN)$ reaction [11–14] have been made at intermediate energies, between 200 and 290 MeV, using polarized protons and polarized ^{3}He targets. These experiments addressed specifically the degree to which the g.s. spin of ^{3}He is determined by the unpaired neutron. The spin-correlation data from the $^3\vec{\mathrm{He}}(\vec{p},pN)$ experiment [13,14] revealed good agreement with free pn scattering variables at sufficiently high momentum transfers $q = 2.5$ fm^{-1}. This result was taken as experimental evidence that the spin of ^{3}He indeed results primarily from the unpaired neutron. At somewhat higher beam energies (220 and 290 MeV) but lower values of q, large deviations were found [11,12] from the free values and plane-wave impulse approximation predictions. These deviations were taken as evidence for significant final-state interactions (FSI) which make an interpretation of the data in terms of Faddeev wave functions and a direct interaction mechanism difficult.

Isoscalar and isovector quasifree responses have been calculated [15–17] using Faddeev wave functions for ^{3}He and GFMC-generated wave functions for ^{4}He. These predictions can now be tested by experiment. Although the separation of the nuclear spin-dependent response into its longitudinal and transverse parts requires the measurement of spin-transfer variables, the measurement of cross sections and asymmetries reported in this paper provides important constraints on theoretical models.

Considering the wealth of (p,n) data and the importance of the study of few-nucleon systems, it is quite surprising that so far no inclusive intermediate-energy (p,n) data for ^{3}He have been published and that data for ^{4}He became available only as part of the experiments [18] described in this paper. A Letter [19] on some of the ^{4}He results has been published recently with emphasis on the astrophysical aspects of that reaction and the question of whether narrow resonances exist in the $p + {}^3$He residual scattering system.

Another motivation for studying the (p,n) reaction on ^{3}He at intermediate energy is the claim, based on the early (p,n) measurements on mass-3 targets below 50 MeV incident energy [20,21] and other work [22–25], that isospin $T = 1/2$ and $T = 3/2$ resonances exist in the three-nucleon system. Data for $^3\mathrm{He}(p,n)$ at intermediate energy, where the reaction mechanism is better understood, may be able to verify or refute the evidence for the three-proton resonance ($T = 3/2$) deduced from the low-energy data.

In this paper, we report the first measurements of the cross sections and analyzing powers for the $^3\mathrm{He}(p,n)$ reaction at an intermediate energy $T_p \approx 200$ MeV. Also we present the inclusive data for the $^4\mathrm{He}(p,n)$ reaction at 200 MeV for comparison with the ^{3}He results. Our double-differential cross section and A_y data cover a range of momentum transfers q between 0 and about 2.2 fm^{-1} and excitation energy E_x up to at least 50 MeV. We present an analysis of these spectra in the framework of the plane- and distorted-wave impulse approximations (PWIA and DWIA, respectively) using a QF scattering model employed in the computer code THREEDEE [26]. Also we obtain single-differential cross sections by integrating the spectra over excitation energy from 0 to 50 MeV as well as asymmetries averaged over this energy range, and compare the results with the free *NN* scattering variables [27] and integrated or averaged THREEDEE predictions.

A brief description of the experimental setup with emphasis on the ^{3}He part of the experiment is given in Sec. II. (The setup has been described in some detail in Ref. [18] and briefly in Ref. [19].) In Sec. III, the experimental results are summarized and discussed in terms of the free *NN* scattering variables and a simple Fermi gas model, including Pauli blocking. An analysis of the data with the QF scattering model employed in THREEDEE [26] is discussed in Sec. IV, and previous work on charge-exchange reactions on mass 3 are reviewed and compared with the results of this work in Sec. V. Conclusions are presented in Sec. VI.

II. EXPERIMENT

The experiment was performed in two separate runs at the Indiana University Cyclotron Facility utilizing the beam swinger and neutron time-of-flight (NTOF) facility [28] at $T_p \approx 200$ MeV. In one experiment, at $T_p = 199$ MeV, neutron time-of-flight spectra were obtained at five angles between 0° and 20° in a neutron detector station located 76 m from the target at a nominal scattering angle of 0°. In the other run, at $T_p = 200$ MeV, data were taken at several angles between 24° and 44° using a detector station located 50 m from the target at the nominal scattering angle of 24°. Six NE102 plastic scintillation detectors, of dimensions 10 cm $\times$ 15 cm $\times$ 100 cm, were positioned longitudinally in a vertical stack in the detector stations. Although there is recent evidence that the cyclotron energy may be lower than the values given above by as much as 1.3%, we have used these energies for the analysis in this work. None of our conclusions are affected by this uncertainty in incident energy.

The neutron energy resolution was about 600 keV [full

width at half maximum (FWHM)] in the detectors at 0° and approximately a factor of 2 worse at 24°. By varying the beam swinger magnets we obtained spectra in an angular range from 0° to 44° in about 5° steps. Cyclotron pulse selection was chosen such that the measurable range of excitation energy E_x extended from 0 to about 60 MeV. In the analysis of the experimental data, we applied a high software pulse-height threshold to the signals from the scintillation detectors in order to eliminate events from ''frame overlap.'' These events arise from slow neutrons from an earlier beam pulse. In addition, this pulse-height threshold essentially eliminated residual backgrounds arising from cosmic rays. The analyzing powers A_y were measured using protons of average polarization $\approx 73\%$ (normal to the reaction plane).

For the purpose of energy and neutron efficiency calibrations, we took spectra with solid ^{12}C and ^{13}C targets at $T_p \approx 200$ MeV and at two other incident energies, $T_p \approx 100$ and 147 MeV. The relative efficiency of the neutron detectors was determined empirically by normalizing measured yields from the ^{12,13}C(p,n) reactions at all three incident energies to published cross sections at similar incident energies [29–33]. The energies of peaks corresponding to well-known states in ^{12}N and ^{13}N were used for neutron energy calibration.

For the measurements on ^{3}He and ^{4}He, a high-pressure, low-temperature gas target was developed. This target was operated near liquid-nitrogen temperature (77 K) and at absolute pressures up to 7 atm. The cell temperature and pressure were continuously monitored during the experiment. Typical areal densities were ≈ 12 mg/cm^2 for ^{3}He (but only 5.8 mg/cm^2 at 0°) and ≈ 18 mg/cm^2 for ^{4}He. The gas cell windows were made of 25.4-μm-thick Havar foil. Background (empty-target) spectra were taken at the same angles as the spectra with the gas-filled target. We also measured spectra with $^{13}CH_4$ in the target cell (at room temperature and a pressure of ≈ 4 atm) for comparison with the solid ^{13}C target data. After correcting for the difference in areal density of the solid and gaseous targets, these spectra agreed to within the systematic uncertainties associated with the areal density of the gaseous target ($\approx 5\%$), suggesting that the performance of the gaseous target is well understood.

Excitation energy spectra were constructed from the time-of-flight spectra. For the ^{3}He(p,n) reaction, the excitation energy $E_x = 0$ of the three-proton system was chosen to be at the three-proton rest mass energy. For the ^{4}He(p,n) reaction, $E_x = 0$ in ^{4}Li* was set to be at the $p + ^3$He rest mass energy. Figure 1 shows typical energy spectra taken at $T_p \approx 200$ MeV for ^{3}He(p,n) with a full (line histogram) and an empty target (bar histogram) at $\theta_{lab} = 5°$ (top panel) and 20° (bottom panel).

In both the empty- and full-target spectra at 5°, narrow peaks are observed at $E_x \approx 0$ and 12 MeV and a broad structure is seen centered near 16 MeV. These structures result from transitions to Gamow-Teller (GT) resonances ($\Delta L = 0, \Delta S = 1$) excited by (p,n) reactions on the nuclei in Havar. The narrow peak at $E_x \approx 9$ MeV is from the ^{12}C$(p,n)^{12}$N$(1^+$, g.s.) reaction on a small carbon contamination on the Havar windows. At 0°, the spectra (not shown) are dominated by these peaks, which are superimposed on the neutron yield from ^{3}He(p,n), making their subtraction using the empty-target spectra difficult. The differential cross

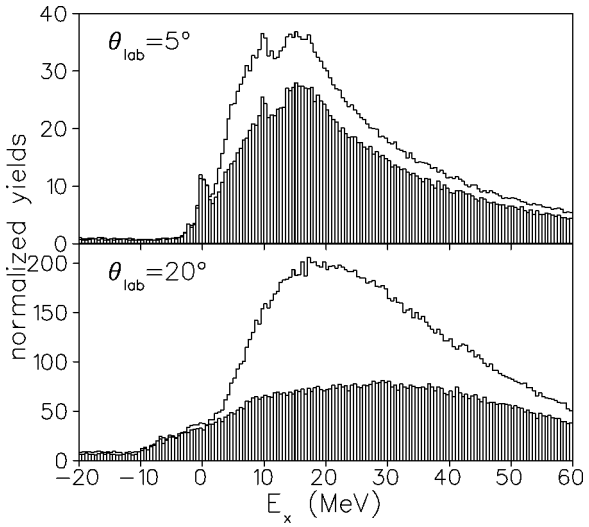

FIG. 1. Typical spectra taken at $T_p = 200$ MeV with an empty target (bar histograms) and a target filled with ^{3}He gas (line histograms) at $\theta_{lab} = 5°$ and 20°. The narrow peaks at $\theta_{lab} = 5°$ are from (p,n) reactions on the elements in Havar and on a carbon contamination (see text).

sections of the GT resonances decrease rapidly with increasing angle [34] and at angles larger than 10° the yields from reactions on Havar are from transitions to continuum states, which create a flat background under the yields from helium. This flat background was then subtracted easily for both ^{3}He (Fig. 1, bottom panel) and ^{4}He targets.

For ^{3}He, the signal-to-background ratio, integrated from $E_x = 0$ to 50 MeV, increases from about 1:6 at $\theta_{lab} = 0°$ to 2:1 at intermediate angles (near 16°) where the ^{3}He(p,n) cross section reaches its maximum, and then decreases with increasing angle to 1:3 at 40°. The signal-to-background ratio for ^{4}He, 1:1 at small angles and 4:1 at the cross section peak, was significantly better for two reasons. First, in the ^{4}He(p,n) spectra, the background peaks are located below the reaction threshold where they do not interfere with the yield from ^{4}He because the Q value for ^{4}He$(p,n)p^3$He is much more negative (-20.59 MeV) than for ^{3}He$(p,n)3p$ (-7.72 MeV). Second, the (p,n) cross sections for ^{4}He are approximately 2 times larger than for ^{3}He.

Generally, the normalized yields from empty and full targets match very well at E_x below threshold ($E_x \leq 0$ MeV). Thus the double-differential cross section spectra (Figs. 2 and 3 in the next section), obtained from the background-subtracted yields, show essentially zero cross section in that region. The error bars in the two figures represent only the statistical uncertainties. Not included in the error bars is an approximately 8% systematic uncertainty in absolute cross sections which is primarily due to the uncertainties in the neutron detector efficiency and the areal density. At 0°, where the signal-to-background ratio is the smallest (about 1:6 for ^{3}He and 1:1 for ^{4}He), there is an indication of nonzero yield below $E_x = 0$ MeV in the spectra. We estimate an additional 5%–10% systematic uncertainty associated with background subtraction difficulties peculiar to this angle.

We conclude the current section with a brief discussion of the uncertainties in the asymmetries. The experimental spectra of the asymmetries, for both ^{3}He(p,n) and ^{4}He(p,n) at

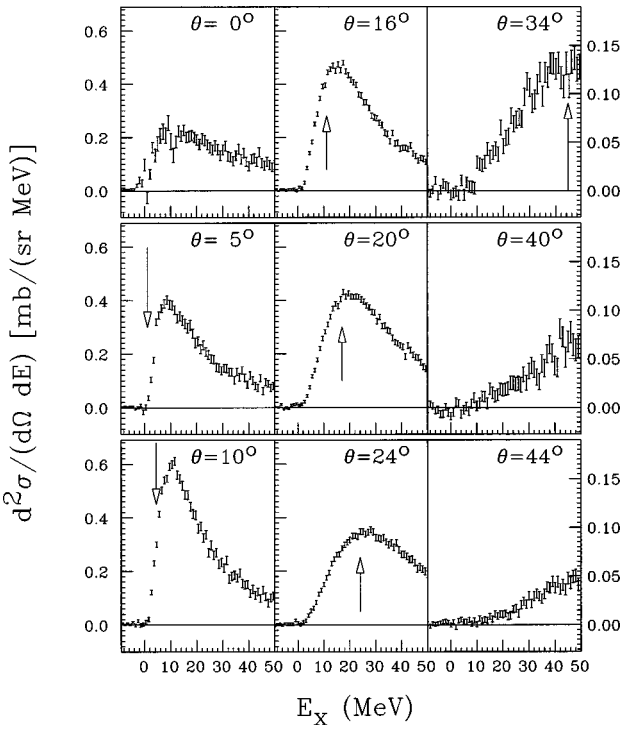

FIG. 2. Double-differential cross sections $d^2\sigma/(d\Omega\ dE_x)$ for the ^{3}He(p,n) reaction at $T_p=200$ MeV between $\theta_{\rm lab}=0°$ and 44°.

six selected angles each (not including 0°), are presented and discussed in Sec. IV (PWIA and DWIA analyses). Also presented there are excitation-energy-averaged asymmetries at all scattering angles. The uncertainties shown in the asymmetry figures include statistical uncertainties as well as an estimated 3% uncertainty in the measured beam polarization.

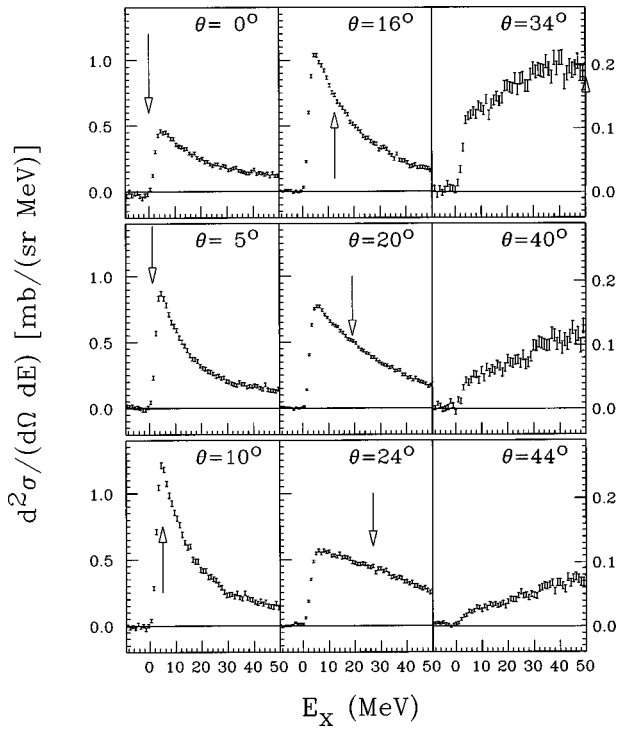

FIG. 3. Double-differential cross sections $d^2\sigma/(d\Omega\ dE_x)$ for the ^{4}He(p,n) reaction at $T_p=200$ MeV between $\theta_{\rm lab}=0°$ and 44°.

We note that at 0° the asymmetry must be zero. Indeed, for ^{4}He(p,n), this expected value lies within one standard deviation of the experimental value for the averaged asymmetry (see Fig. 12 in Sec. IV), indicating that there is no large systematic error associated with the A_y measurements. For ^{3}He(p,n), the averaged asymmetry at 0° is about one standard deviation removed from zero. The large uncertainty in the averaged A_y for ^{3}He(p,n) at 0° is due to the limited statistics at this angle where the signal-to-background ratio is 1:6.

III. EXPERIMENTAL RESULTS

A. Energy spectra of cross sections and asymmetries

Double-differential cross sections in the laboratory (energy spectra) from the ^{3}He(p,n) reaction at nine angles in the angular range from 0 to 44° are displayed in Fig. 2 as a function of excitation energy E_x in the residual three-proton system (with $E_x=0$ at the three-proton rest mass energy). The spectra are dominated by a broad peak that moves systematically to higher E_x with increasing scattering angle (momentum transfer q) as expected for QF scattering. At small momentum transfers ($\theta_{\rm lab}\leqslant 16°$ or $q\leqslant 0.90$ fm^{-1}) for the ^{3}He(p,n) reaction, the peak shape near threshold is affected strongly by the phase space factor which rises rapidly from 0 at threshold. At larger q ($\theta_{\rm lab}\geqslant 34°$ or $q\geqslant 1.79$ fm^{-1}) a significant part of the QF peak lies beyond the limits in excitation energy, imposed by the experimental time-of-flight window. At intermediate q ($16°\leqslant\theta_{\rm lab}\leqslant 40°$ or 0.90 fm$^{-1}\leqslant q\leqslant 2.05$ fm^{-1}), the maxima in the spectra are found near the calculated positions of the QF scattering centroids indicated by the arrows. The widths of the peaks are consistent with values expected from the Fermi motion of the nucleons in the targets. Both observations strongly favor the conclusion that the ^{3}He(p,n) reaction at incident energies of about 200 MeV is dominated by the QF scattering process.

The positions of the arrows were calculated with the nonrelativistic equation $E_x(\text{centroid})=(q^2/2m)\times\frac{2}{3}$ for ^{3}He(p,n) and $E_x(\text{centroid})=(q^2/2m)\times\frac{3}{4}$ for ^{4}He(p,n). Here q is the momentum transfer for free NN scattering at 200 MeV and m is the nucleon mass. The factors $\frac{2}{3}$ and $\frac{3}{4}$ transform the kinetic energy of the proton (after charge exchange) in the laboratory system to the ''excitation energy'' E_x of the residual scattering state, that is, $p+(2p)$ for ^{3}He(p,n) and $p+{}^3$He for ^{4}He(p,n).

At 10° and below, the double-differential cross sections for ^{3}He(p,n) show a pronounced maximum near $E_x=10$ MeV. This maximum in the differential cross section is most likely caused by the sharp cutoff of the QF scattering distribution by phase space as E_x approaches threshold. The yield near $E_x=10$ MeV peaks at 10° and decreases rapidly with increasing angle as the maximum in the yield slowly moves to higher E_x in better agreement with the values indicated by the arrows. If the broad peak near 10 MeV at small angles were the result of a resonance in the three-proton system near that energy, a peak of similar width (but most likely much reduced yield) should also be seen near 10 MeV at larger angles $\theta_{\rm lab}\geqslant 24°$, but none was observed there. At these larger angles, the smooth increases in the experimental yields between threshold and the QF centroid are in good agree-

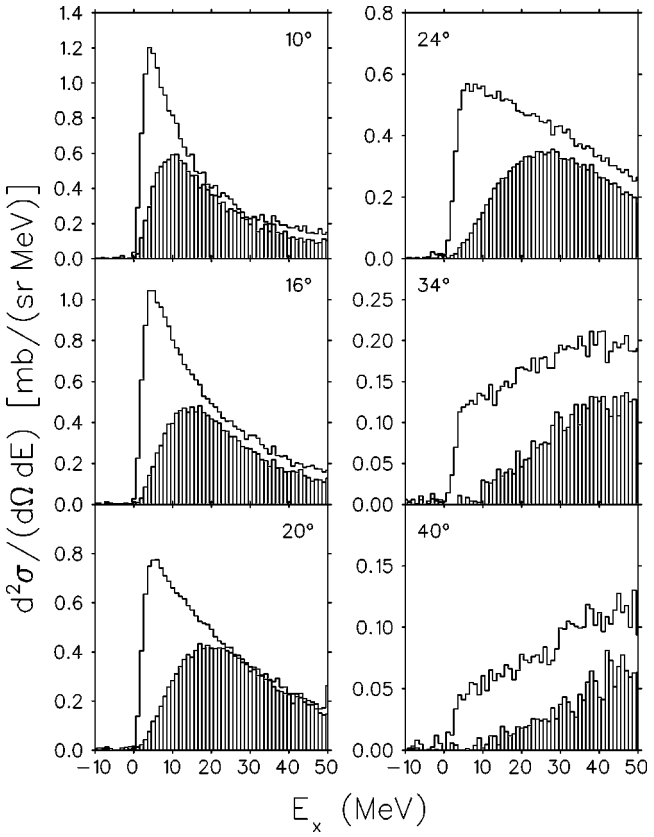

FIG. 4. Double-differential cross sections at six angles for both ^{3}He (bar histograms) and ^{4}He (line histograms).

ment with the shapes expected for a QF peak. (See PWIA and DWIA analyses discussed below.)

Figure 3 displays energy spectra from the ^{4}He(p,n) reaction as a function of excitation energy in the mass-4 system (with E_x of ^{4}Li* equal to zero at the ^{3}He$+p$ rest mass energy). In contrast to the ^{3}He results, the spectra from ^{4}He(p,n) show a steep rise near threshold at *all* scattering angles. At forward angles ($\leqslant 16°$), there is a pronounced peak at $E_x \approx 4$ MeV, as expected from the excitation of the low-lying resonances in ^{4}Li [25] of orbital angular momentum $L=1$ and spin and parity $J^\pi = 0^-$, 1^-, and 2^-.

The yield at E_x beyond the peak near threshold falls off exponentially but the slope becomes less negative with increasing angle up to 24° and at $\theta \geqslant 34°$ the cross sections rise with increasing E_x. At $\theta = 34°$, the yields reach a maximum near the predicted energy of the QF scattering centroid indicated by the arrow. We show in Sec. IV below that both the resonance behavior of the ^{4}He(p,n) spectra near threshold and the continuum at higher E_x can be described by a QF scattering model that uses a sequential-coordinate formalism.

The apparent larger width of the QF continuum for ^{4}He(p,n) than for ^{3}He(p,n) is due in part to the larger Fermi momentum of the nucleons in ^{4}He than in ^{3}He. The spectral distribution for ^{4}He(p,n) is broadened also by the strong $L=1$ resonances centered near 4 MeV excitation in ^{4}Li. In order to facilitate the comparison between the spectra from ^{3}He and ^{4}He we have overlaid the energy spectra at six angles in Fig. 4. Clearly, the prominent resonance behavior of the ^{4}He(p,n) spectra near threshold is absent in the spectra from ^{3}He(p,n). This comparison of the spectral shapes

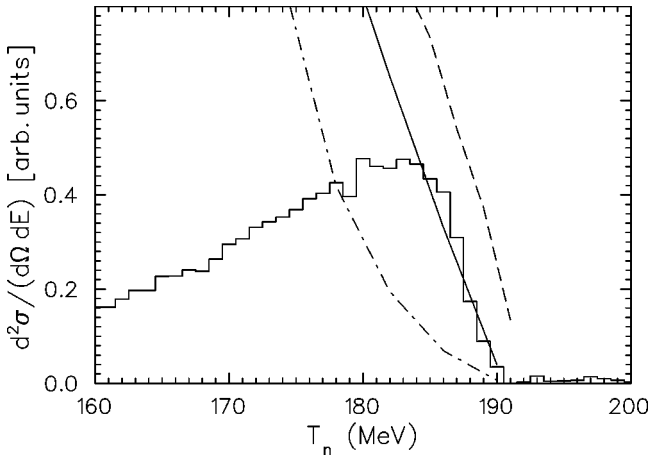

FIG. 5. Phase space spectra at $T_p = 200$ MeV, $\theta_{\rm lab} = 5°$, obtained with FOWL [35]. Dot-dashed line, three-body (^{2}He$+p+n$) phase space; dot-dashed line, four-body ($p+p+p+n$) phase space; solid line, four-body ($p+p+p+n$) phase space with $^1S_0$ FSI's between the two protons of small relative momenta.

from the ^{3}He(p,n) and ^{4}He(p,n) reaction, and the analysis of the data in the framework of the DWIA (see Sec. IV), leads us to conclude that the ^{3}He(p,n) reaction proceeds exclusively by simple QF scattering with no indication of a $p+2p$ (^{3}Li) resonance affecting the spectral shapes.

We performed phase space calculations using the CERN code [35] in order to analyze the spectra near threshold where the phase space factor dominates the spectral shapes. For the ^{3}He(p,n) reaction we found that the rise of the yield near threshold at small angles is reproduced better by three-body (dashed line) than four-body (dash-dotted line) phase space calculations (Fig. 5). This result is expected because the two protons in the g.s. of ^{3}He are in a relative $^1S_0$ state and, to first order, the $n(p,n)p$ QF scattering occurs on the unpaired neutron only whereas the $^1S_0$ diproton (which we will call ^{2}He) acts as a spectator. Thus, there are effectively three particles in the final state $n+p+^2$He, and use of three-body phase space is appropriate. Compared to experiment, four-body phase space predictions rise much too slowly with E_x.

FOWL allows the use of a kinematics-dependent weight factor which may be employed, for example, to include a final-state interaction between two protons in the four-body final state. The FSI between two protons is known to be important when the relative momenta are small, i.e., near threshold, $E_x \approx 0$ MeV. We used the parametrization of the $^1S_0$ two-proton FSI of Ref. [36] and found that its inclusion in a four-body phase space calculation partially restores the spectrum to that predicted by three-body phase space and provides an even better description (Fig. 5, solid line) of the near-threshold data from ^{3}He(p,n) than the three-body phase space spectrum.

B. Angular distributions

We integrated the double-differential cross sections $d^2\sigma/(d\Omega\, dE_x)$ for ^{3}He(p,n) and ^{4}He(p,n) over the excitation energy (E_x) range from 0 to 50 MeV and obtained the angular distributions of $d\sigma/d\Omega$ shown in Fig. 6. Note that at the larger angles ($\theta_{\rm lab} \geqslant 34°, q \geqslant 1.79$ fm^{-1}) a significant

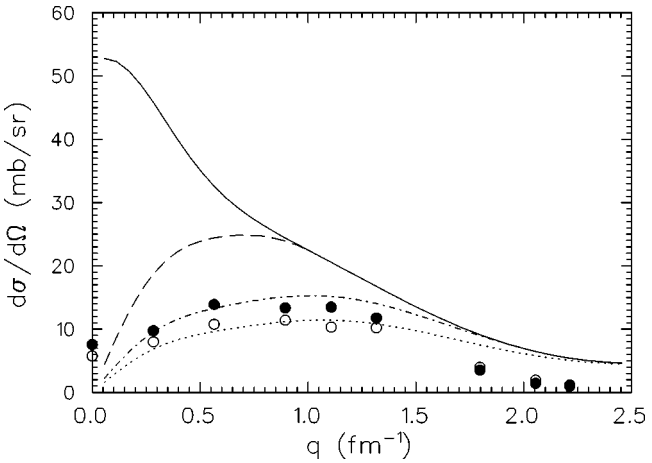

FIG. 6. Single-differential cross sections for ^{4}He(p,n) (open circles) and ^{3}He(p,n) (solid circles) as a function of q obtained by integrating the spectra from 0 to 50 MeV in excitation energy. The data for ^{4}He were divided by a factor of 2 to facilitate comparison with ^{3}He. Uncertainties are smaller than plotting symbols. The solid line is the free NN charge-exchange cross section from SAID [27]. Results of the Fermi gas model calculations with Pauli blocking are shown for $p_f = 100$ MeV/c (dashed line), 200 MeV/c (dot-dashed line), and 280 MeV/c (dotted line).

part of the QF continuum lies outside the experimental limits. We did not attempt to extrapolate the peak shapes into the unmeasured region.

The single-differential cross sections for ^{3}He(p,n) are expected to be about a factor of 2 smaller than for ^{4}He(p,n) because there is only one neutron in ^{3}He versus two in ^{4}He; therefore the cross sections for ^{4}He(p,n) were renormalized by a factor of 0.5 to facilitate the comparison with the ^{3}He(p,n) data in Fig. 6. Indeed, the renormalized cross sections for ^{4}He(p,n) (open circles) are within about 20% of those for ^{3}He(p,n) (solid circles). This result is somewhat unexpected since spectral shapes for the two targets differ considerably in the excitation energy region near threshold (Fig. 4). It appears that the very strong FSI in the p^3He channel (from ^{4}Li* resonances) merely redistributes the total yield over E_x.

Also shown in Fig. 6 (solid lines) are the differential cross sections for free nucleon-nucleon charge exchange deduced from np elastic scattering [27]. The free cross sections are much larger than the ^{3,4}He(p,n) data at small angles ($\theta_{\rm lab} \leqslant 16°, q \leqslant 0.90$ fm^{-1}). The data approach about 3/4 of the free values near 24° ($q \approx 1.31$ fm^{-1}) but the disagreement widens again as the scattering angle is increased. The latter discrepancy is due partly to the limits on the experimental energy range which exclude up to one-half of the expected yield as is apparent in the spectra (Figs. 2 and 3).

The large discrepancies between the free values and the excitation-energy-integrated cross sections at small angles result from Pauli blocking. As pointed out above, because the dominating configuration in the g.s. of both targets has two protons in the fully symmetric S state, the (third) proton from the (p,n) charge exchange is prevented from occupying a $1s$ state and thus needs to be placed into a $1p$ (or higher) quantum state; therefore, the forward-angle cross sections, which are usually dominated by $\Delta L = 0$ transfer, are strongly suppressed.

The effect of Pauli blocking on the energy-integrated cross section can be parametrized by the q-dependent factor $P(q)$ which renormalizes the free pn cross sections. $P(q)$ can be calculated in a simple Fermi gas model as a function of Fermi momentum p_f and momentum transfer q [37]:

$$P(q) = \frac{3}{4}\frac{q}{p_f}\left[1 - \frac{1}{12}\frac{q^2}{p_f^2}\right] \quad \text{if } q \leqslant 2p_f. \tag{1}$$

The free NN cross sections from Ref. [27] multiplied by $P(q)$ for three different values of p_f are displayed in Fig. 6. The dash-dotted curve calculated with $p_f = 200$ MeV/c reproduces the ^{4}He data (open circles) best whereas the ^{3}He data (solid circles) are fit better with $p_f = 280$ MeV/c. The need for a larger p_f for ^{3}He than ^{4}He is contrary to expectations. This result is not surprising because we are applying theory involving averaging over many nucleons to such light targets. Thus the predictions should be viewed with extreme caution.

Differences between free and QF cross sections may result also from the radial dependence of the nuclear form factor and optical potential distortions. In Sec. IV we discuss DWIA calculations, employing properly chosen optical model potentials, that reproduce the suppression of the forward-angle cross sections obtained here by including Pauli blocking.

IV. PWIA AND DWIA ANALYSIS

In order to better understand the details of the energy spectra and to enlarge the heretofore qualitative discussion of QF scattering, calculations were performed using the code THREEDEE [26]. This code assumes a QF scattering mechanism and employs the DWIA. Initial- and final-state scattering wave functions are described in terms of optical potentials fit to elastic scattering cross sections. This approach is in contrast to treatments of final-state interactions [38,39] in terms of elastic scattering phase shifts which do not specify corresponding wave functions in the interior of the nucleus. It is this interior region which is important in evaluating the DWIA t matrix.

THREEDEE calculates exclusive differential cross sections and polarization observables for the reaction $A(a;c,d)B$, where $A = b + B$. For comparison with inclusive $A(a,c)$ data, the exclusive observables are integrated over the phase space available to the undetected particle d. The interaction of d (a proton) with the residual core B (^{3}He) is the primary FSI of interest in the ^{4}He$(p;n,p)^3$He reaction.

The THREEDEE [26] formalism employs the amplitude factorized DWIA, in which the two-body elastic scattering t matrix and the distorted-wave matrix element enter in the overall scattering amplitude as multiplicative factors. The two-body t matrix is required for the $b(a,c)d$ reaction and should properly be off the mass shell. Two asymptotic formulations are provided for the computation of the t matrix: the initial and final energy prescriptions (IEP and FEP, respectively). The distorted wave matrix element is constructed from the incoming and outgoing nucleon distorted waves, and from the bound nucleon single-particle wave function in the target nucleus.

In THREEDEE, antisymmetrization is taken into account

only to a limited extent. Exchange between the particles a and b is taken into account through the use of a fully antisymmetric $b(a,c)d$ two-body t matrix. Exchange between particle b and B is taken into account through the use of fully antisymmetric wave functions for the target and residual nuclei, together with the usual fractional parentage techniques [40] in generating the necessary spectroscopic factors.

Exchange effects between the projectile a and the core B are explicitly excluded so that the projectile must be among the emitted nucleons. Because the optical potentials fit elastic scattering data, they implicitly include the effect of Pauli blocking on the elastic scattering wave functions; however, the use of an optical potential description for such light targets is somewhat open to question. Nevertheless, because the use of phenomenological optical potentials results in reasonable fits to the forward-angle (p,n) cross sections (see below), it appears that these potentials simulate to some extent the effects of Pauli blocking.

The ''symmetric-coordinate'' formalism [41] used in THREEDEE is appropriate for typical QF scattering experiments, in which the ejected particles c and d are of similar energy. In this formalism, the two outgoing particles c and d are treated equivalently, with the outgoing scattering state wave functions constructed as a function of the relative coordinates $\vec{r}_{cB}$ and $\vec{r}_{dB}$. The momentum operators in the Hamiltonian are then determined from the momenta conjugate to these coordinates. It should be noted that the separation of the final-state three-body wave function into a product of two scattering wave functions depends upon the treatment of a kinematic coupling term $\nabla_c \cdot \nabla_d / B$. Clearly, such a term can be expected to be insignificant for heavy targets. It is also reduced in importance for opening angles close to 90°. In all THREEDEE calculations using symmetric coordinates, the coupling term is approximated by the corresponding asymptotic value.

In the exclusive ^{4}He$(p;n,p)^3$He reaction, a in $A(a;c,d)B$ is the projectile proton, b in $A=b+B$ is a target neutron, and c and d are the ejectile neutron and proton, respectively. Near the $d+B$ threshold ($E_x=0$), the ''scattered'' particle c is a relatively high-energy neutron and the other ejected particle d is a relatively low-energy proton. In such a kinematic region the conjugate momenta of the symmetric-coordinate formalism do not lead to a proper relationship between the value of E_x and the relative energy of particle d with respect to particle B. As a result, there are contributions to the spectra at a fixed value of E_x from a range of relative $d+B$ (e.g., $p+^3$He) energies; for the reaction on ^{4}He, for example, the ejected particle d (a proton) moves away from the residual B (^{3}He) much more slowly than does particle c (the neutron), giving the reaction a sequential quality. Clearly, particles c and d should *not* be treated equivalently. Indeed, the $d+B$ system may even be best described as a resonance of the $X=d+B$ system.

In order to improve our description in this kinematic region, we have modified THREEDEE so that a fixed excitation energy E_x is associated with a unique value of the relative $d+B$ kinetic energy. To achieve this we have adopted a ''sequential-coordinate'' formalism in which the outgoing three-body scattering wave function is constructed as a function of the relative coordinates $\vec{r}_{cX}$ and $\vec{r}_{dB}$ together with the corresponding conjugate momentum operators. Although there is no longer any kinematic coupling, one additional approximation is needed. Specifically, the potential terms in the three-body Hamiltonian are $V_{cB}(\vec{r}_{cB})+V_{dB}(\vec{r}_{dB})$ which preclude separation of the wave function into a product form; however, we adopt the ansatz $V_{cB}(\vec{r}_{cB}) \approx V_{cX}(\vec{r}_{cX})$ which then leads to separation of the wave function into a product of scattering wave functions describing $d+B$ and $c+X$, respectively.

The use of these coordinates permits a correct treatment of resonant structure in the $d+B$ system to the extent that it is included properly in the optical-potential parameterization and, thus, a better description of any structure in the resulting E_x spectra. For all the calculations discussed below, the sequential-coordinate formalism has been used. A similar, though less rigorous, modification of has been employed successfully in the analysis of ^{4}He$(\pi;\pi,p)$ [42] and ^{4}He(p,n) [18,43] data.

For the DWIA calculations, the optical potentials of Refs. [44–48] were employed. These potentials fit elastic scattering data for proton scattering from ^{2}H, ^{3}He, and ^{4}He over several different ranges of incident energies. The exchange term of Ref. [44] was not included in our calculations, an omission that is not expected to affect forward-angle charge-exchange observables. Because the inclusion of an imaginary potential in the $d+B$ channel is relevant only if the proton is observed in the final state [49], the imaginary potential in the $d+B$ channel is set identically set to zero for all calculations. The effective two-body t matrix was constructed from the free NN phase shifts [27]. The standard version of the code obtains the NN phase shifts from [27] at energies between 25 and 800 MeV. We modified the code in order to extend this range of energies down to 2 MeV.

The radial dependence of the $b+B$ bound state wave functions was of the Eckart type [50] for the ^{3}He g.s. and of the variational type [51] for the ^{4}He g.s. In order to limit numerical integrations, our calculations were restricted to the kinematics corresponding to the lowest energies in the residual systems, the diproton (or ^{2}He) and the $J=1/2$ g.s. of ^{3}He. We have assumed $1s$-shell sum-rule-limit values for the spectroscopic factors, i.e., 1 for ^{3}He and 2 for ^{4}He, and have considered only transitions from the $1s$ shell. As a result, we may progressively underestimate the inclusive yield with increasing excitation energy.

The integration over phase space available to the unobserved proton was conducted from $-180°$ to $+180°$ in the scattering plane and from 0° to 60° above the scattering plane. The resulting cross sections were then multiplied by a factor of 2 to account for the region below the scattering plane.

The results from the ^{3}He calculations using the code THREEDEE [26] with all nuclear and Coulomb potentials set to zero (the PWIA calculations) are shown in Fig. 7 for six laboratory scattering angles as dashed (FEP) and dotted (IEP) lines. The general shapes of the experimental spectra are reproduced quite well: the predicted absolute cross sections, however, are much larger than the data at small angles ($\leqslant 24°$) near threshold.

For the DWIA curves shown in Fig. 7, both the $a+A=p+^3$He and $c+(d+B)=n+3p$ potentials, are the $p+^3$H

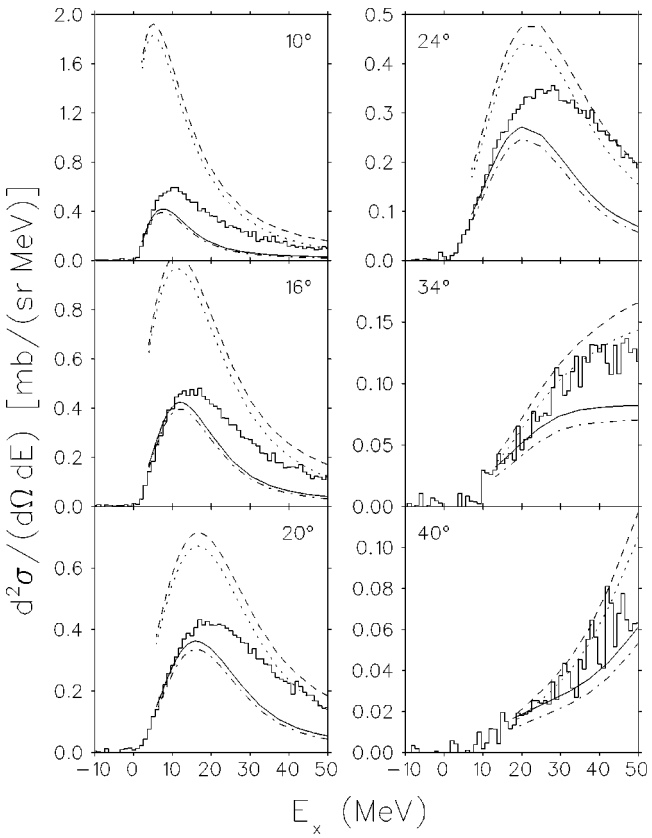

FIG. 7. $d^2\sigma/(d\Omega\ dE_x)$ for the ^{3}He(p,n) reaction at $T_p=200$ MeV between $\theta_{\rm lab}=10°$ and 40°. Data (histogram) and THREEDEE results. PWIA, FEP (IEP) calculations are shown as dashed (dotted) lines and DWIA, FEP (IEP) calculations are shown as solid (dot-dashed) lines. Potentials as specified in text.

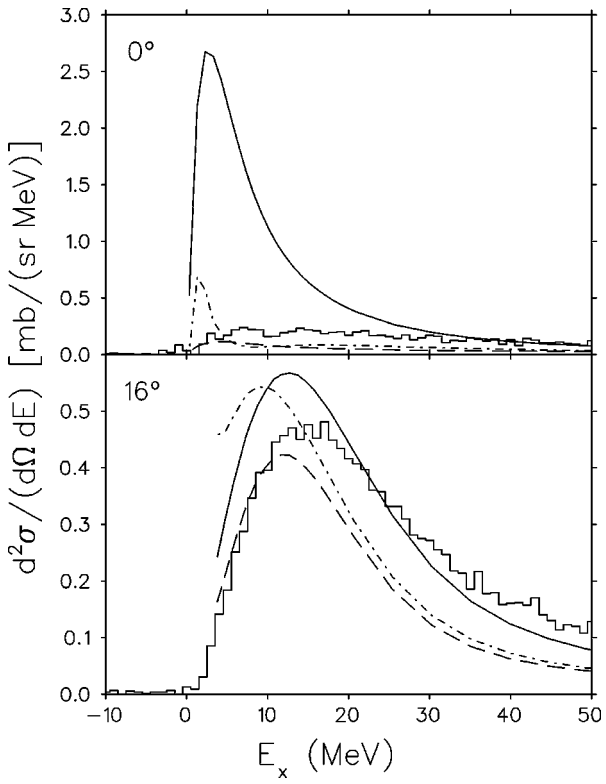

FIG. 8. $d^2\sigma/(d\Omega\ dE_x)$ for the ^{3}He(p,n) reaction at $T_p=200$ MeV at $\theta_{\rm lab}=0°$ (top panel) and 16° (bottom panel). Data (histogram) and THREEDEE results (curves) with different optical potentials for the $p+^2$He channel. Only FEP DWIA calculations are shown. Solid lines with $p+^2$He real (and imaginary) well depth set to zero; long-dashed lines with optical potential of Ref. [45]; dash-dotted lines with optical potential of Ref. [46].

potential of Ref. [44] which contains spin-orbit terms. For the $d+B=p+^2$He channel we used the potential derived [45] from $p+d$ scattering data between 17 and 46.3 MeV. This potential does not have a spin-orbit term.

This choice of optical potentials for the ^{3}He$(p;n,p)^2$He calculations caused a significant decrease in the forward-angle cross sections (solid lines are FEP and dot-dashed lines are IEP), in much better agreement with the data (Fig. 7), especially near threshold and at small angles. At $E_x\geqslant 20$ MeV, the DWIA cross sections are too small at all angles, possibly because two-step processes, not included in THREEDEE, are important for ^{3}He(p,n), or because of uncertainties in the optical potentials, particularly in the $p+^2$He channel; however, both PWIA and DWIA predict the centroids and widths of the measured QF peak reasonably well at all angles.

We investigated the sensitivity of the spectra to the choice of optical potential in the $p+^2$He channel. Setting the real potential depth to zero gives very large cross sections at 0° (Fig. 8, top panel, solid line). There is a prominent peak in the calculated spectra near threshold which is not present in the data. Using the optical potential of Ref. [46] which is based on the analysis of $p+d$ scattering data [52] above 40 MeV, reduces the cross section considerably but there is still an unphysical spike near threshold at 0° (dash-dotted line): however, when the potential of Ref. [45] is used there is no such spike near threshold at 0°, but the predicted cross section is too small (long-dashed line). At 5° this potential gives cross sections in good agreement with the data up to about $E_x=10$ MeV, but too small cross sections above this excitation energy.

At 16° (Fig. 8, bottom panel) and larger angles (not shown), the spectra with the potential of Ref. [46] are shifted to smaller E_x and reproduce the data less well than the other DWIA calculations which use the potential of Ref. [45] or have both real and imaginary depths set to zero. All potentials give too large cross sections at high E_x. The large sensitivity of the absolute cross sections and their E_x dependence on the optical potentials means that it is currently not possible to draw conclusions about medium effects on the elementary NN interaction in ^{3}He(p,n) or about possible contributions from the small components of the wave functions.

The results from the PWIA calculations using the code THREEDEE [26] for ^{4}He are shown in Fig. 9. The predictions are similar to those for ^{3}He(p,n), but most notably the larger Fermi momentum for ^{4}He causes the strength to be distributed over a larger range of E_x; however, as pointed out above, the experimental spectra differ greatly for the two targets. Whereas the ^{3}He spectra show clear QF scattering peaks at angles $\geqslant 16°$, for ^{4}He, there is evidence of a maximum near the excitation energy expected for QF scattering only at 29° (Fig. 9) and at 34° (Fig. 3).

The PWIA calculations for the ^{4}He(p,n) reaction com-

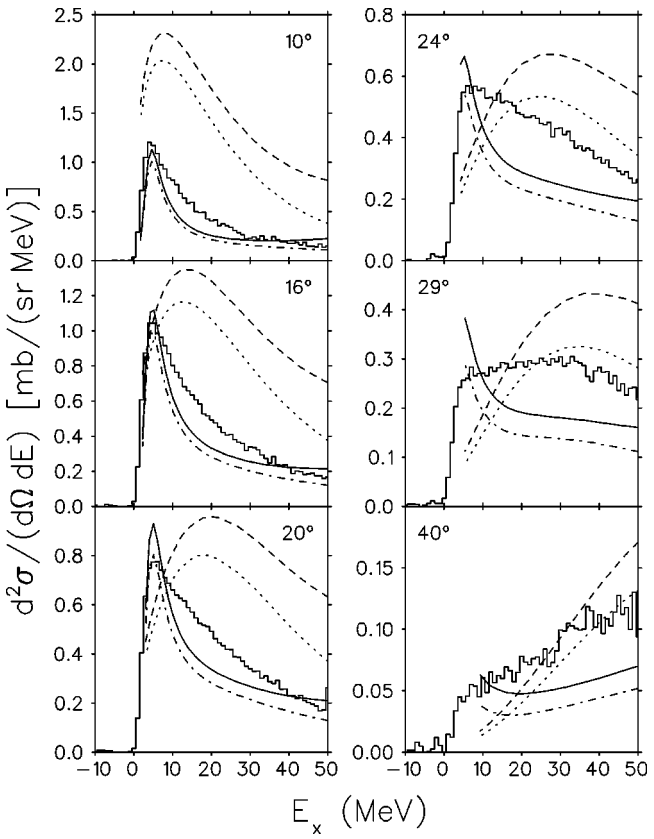

FIG. 9. $d^2\sigma/(d\Omega\ dE_x)$ for the ^{4}He(p,n) reaction at $T_p=200$ MeV between $\theta_{\rm lab}=10°$ and 40°. Data (bar plot) and THREEDEE results. PW FEP (IEP) calculations shown as dashed (dotted) lines. DW FEP (IEP) calculations shown as solid (dot-dashed) lines. Potentials as specified in text.

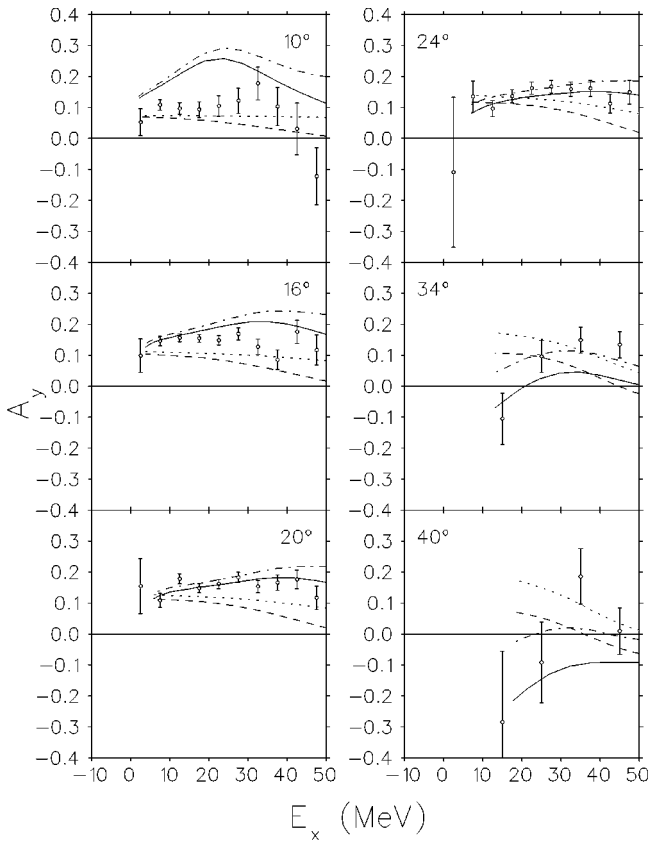

FIG. 10. A_y for the ^{3}He(p,n) reaction at $T_p=200$ MeV between $\theta_{\rm lab}=10°$ and 40°. Data (circles) and THREEDEE results. PW FEP (IEP) calculations shown as dashed (dotted) lines. DW FEP (IEP) calculations shown as solid (dot-dashed) lines. Potentials as specified in text.

pletely miss the resonant structure in ^{4}Li* near threshold. For the DWIA curves shown in Fig. 9, the $a+A=p+^4$He potential is taken from Ref. [47], the $c+(d+B)=n+^4$Li potential is the $p+^4$He potential of Ref. [44], and the $d+B=p+^3$He potential is taken from Ref. [48], again with the imaginary part set to zero. Essential for the fit to the resonant structure near threshold is the use of sequential kinematics and of the $p+^3$He potential [48] which has a strong $L=1$ potential resonance near the energy of the negative parity states [25] of ^{4}Li (0^-, 1^-, and 2^-).

The strong cross section enhancement in ^{4}He(p,n) near threshold is reproduced quite well by the DWIA at almost all angles. At higher excitation energies and large angles the experimental cross section is underestimated, possibly indicating contributions from multiple scattering which may be more important than for the ^{3}He target. The shapes of the IEP cross sections are similar to the corresponding FEP shapes, but the differences between FEP and IEP in magnitude are larger for ^{4}He than ^{3}He owing to the larger neutron binding energy in ^{4}He.

The calculated analyzing powers A_y from THREEDEE [26] for ^{3}He and the measured values are shown in Fig. 10. The PWIA results resemble the data reasonably well but the asymmetries from the DWIA calculations are too large at $\theta_{\rm lab}\leqslant 16°$ with the potential of Ref. [45]. At these small angles the A_y calculated with the potential of Ref. [46] (not shown) reproduce the data quite well but too large cross sections were predicted at forward angles. Without spin-orbit terms in all channels, the A_y are indistinguishable from the PWIA results. The cross sections are essentially unaffected by the spin-orbit terms.

The A_y for ^{4}He are shown in Fig. 11. The PWIA results resemble the data only in their general E_x dependence, but are roughly a factor of 2 too small at small momentum transfers; however, the DWIA predictions reproduce the data reasonably well in both their magnitude and E_x dependence. At large angles, 24° and 29°, there is a preference for using the IEP kinematics in the two-body t matrix. This choice would be consistent with the analysis of $(p,2p)$ kinematics in Ref. [53] based upon a Faddeev description.

The double-differential cross sections $d^2\sigma/(d\Omega\ dE_x)$ from THREEDEE were integrated over E_x from threshold to $E_x=50$ MeV for comparison with the angular distribution of the integrated experimental spectra for both ^{3}He and ^{4}He (Fig. 12). As already mentioned, the E_x-integrated experimental cross sections for the two targets have similar angular dependence. In particular, both targets exhibit the strong Pauli-blocking effects near 0°. The shapes of the THREEDEE angular distributions for both ^{3}He and ^{4}He agree reasonably well with the data, despite the complication that at angles $\geqslant 34°$ both theory and experiment include only about one-half of the quasifree peak; however, at the peak of the angular distribution, the absolute cross sections from THREEDEE are too small by about a factor of 1.2 for ^{4}He and a factor of

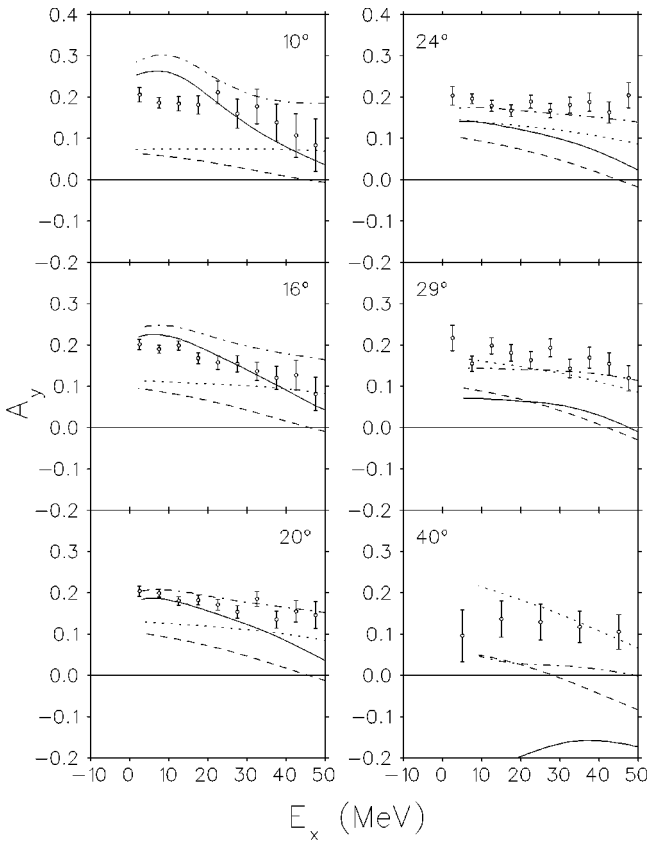

FIG. 11. A_y for the ^{4}He(p,n) reaction at $T_p=200$ MeV between $\theta_{\rm lab}=10°$ and 40°. Data (circles) and THREEDEE results. PW FEP (IEP) calculations shown as dashed (dotted) lines. DW FEP (IEP) calculations shown as solid (dot-dashed) lines. Potentials as specified in text.

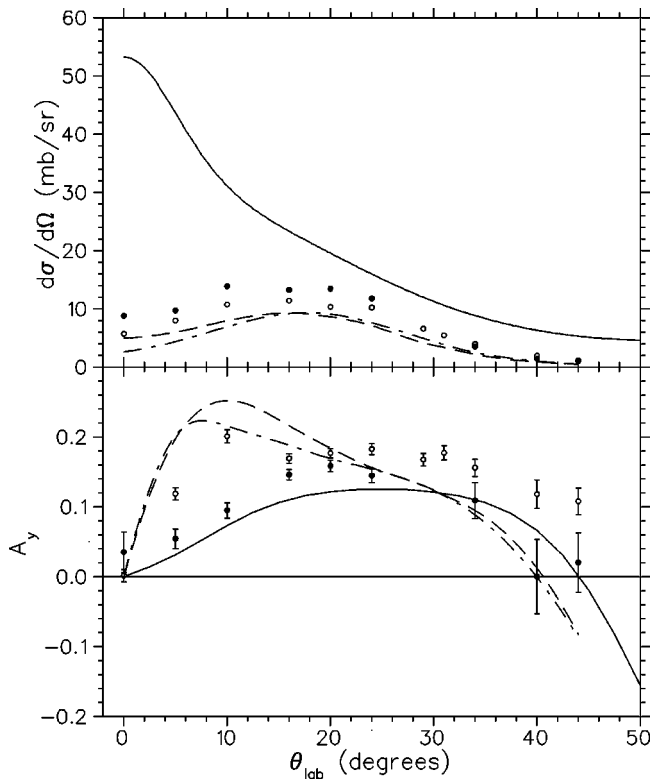

FIG. 12. Single-differential cross sections (laboratory) (top panel) and excitation-energy-averaged asymmetries (bottom panel) for ^{3}He(p,n) (solid circles) and ^{4}He(p,n) (open circles) at $T_p=200$ MeV as a function $\theta_{\rm lab}$. [Same cross section data as shown in Fig. 6. As in Fig. 6, the cross sections for ^{4}He(p,n) were multiplied by a factor of 0.5.] Calculated curves are integrated cross sections and averaged asymmetries from THREEDEE. Short dot-dashed lines, ^{3}He FEP, short dashed lines, ^{4}He FEP. The solid lines are from SAID [27] as in Fig. 6.

1.7 for ^{3}He. Recall that THREEDEE gives too small double-differential cross sections at high E_x. We attributed this discrepancy to either multiple scattering or an uncertainty in the choice of optical potential, especially in the $p+^2$He channel. [Both THREEDEE cross sections and data for ^{4}He(p,n) are multiplied by a factor of 0.5 for this plot.]

The A_y from THREEDEE for both ^{3}He and ^{4}He, averaged over 0–50 MeV, are shown in Fig. 12, bottom panel. At small angles, the calculations for ^{4}He(p,n) reproduce the observed enhancement of A_y over the free NN values. But the lack of such an enhancement in the ^{3}He(p,n) data is reproduced only with the $p+^2$He potential of Ref. [46] (not shown) which does not fit the forward-angle cross sections. The agreement between ^{4}He(p,n) data and calculations degrades with increasing angle where the cross sections are small. The forward-angle enhancement of the A_y for ^{4}He(p,n) is in contrast to the usually good agreement between data and free values observed in work [2] on p-shell nuclei at 186 MeV, on ^{12}C at 495 MeV [3], and in our ^{3}He(p,n) data, and also to the suppression of A_y seen in ^{12}C(p,n) at 795 MeV [3].

The failure of the DWIA to fit the forward-angle A_y for ^{3}He(p,n) whereas the cross sections are reproduced reasonably well with the potential of Ref. [45], might indicate that the DWIA calculations for ^{3}He(p,n) have a significant deficiency. In addition to the use of possibly unsatisfactory optical potentials one might question indeed the use of a distorted-wave description at all for such a light target.

Thus far, we carried out calculations only for the fully symmetric S-state components of the target g.s. (which for ^{3}He is of the order of 90% of the total). In view of this simplification of the treatment of the spin structure in the calculations with THREEDEE, we cannot currently determine the sensitivity of the predictions to the spin structure. In the case of ^{3}He, experiments using polarized beams [10] and polarized beams and targets [11–14] have been completed and analyses are underway which include descriptions both of the rich spin structure of the target and the unbound two-proton residual nucleus.

V. DISCUSSION OF PREVIOUS WORK ON ^{3}He AT LOWER ENERGY

As mentioned briefly in the Introduction, claims have been made regarding the existence of $T=1/2$ and $T=3/2$ resonances in the mass-3 system. Reference [20] deduced evidence for a $T=1/2$ resonance at $E_x=9.6\pm0.7$ MeV in ^{3}He from inclusive neutron spectra of the ^{3}H$(p,n)^3$He reaction at $T_p=30$ MeV: a $T=1/2$ resonance was also deduced, however, at the higher energy $E_x=14.2$ MeV, by a phase shift analysis of $p+d$ elastic scattering [24]. The existence of this resonance is supported by a theoretical study of the three-nucleon system [54].

Evidence for a $T=3/2$ (three-proton) resonance was obtained [20] from a ^{3}He(p,n) neutron spectrum measured with 48.8-MeV protons. The maximum of the enhancement was found near an excitation energy $E_x=9\pm1$ MeV ($\Gamma=10.5$ MeV) in the three-proton system (where $E_x=0$ at the three-proton rest mass energy). An enhancement observed by the same authors [20] in the spectra from ^{3}H$(p,n)^3$He, centered near $E_x=16\pm1$ MeV in ^{3}He ($\Gamma=9$ MeV), was attributed tentatively to a $T=3/2$ resonance, the isobaric analog of the claimed three-proton resonance deduced from their ^{3}He(p,n) data.

Reference [21] and, more recently, Ref. [55] found deviations from the four-body phase space in the neutron spectrum from ^{3}He(p,n) below the four-body end point energy ($E_x \geqslant 0$), which were tentatively attributed to a $^1S_0$ two-proton FSI and not a three-proton resonance. The importance of the $^1S_0$ two-proton FSI at forward angles is well established in the inclusive neutron spectra from the ^{2}H$(p,n)2p$ reaction [56]; however, as we discussed in the Introduction, in the case of ^{3}He the two target protons with their spins antiparallel form already the $^1S_0$ state in the target. Thus, in the impulse approximation, the (p,n) reaction occurs on the unpaired neutron only and the two ($^1S_0$) target protons are a ''spectator'' ^{2}He. The final state consists of the detected neutron, the ^{2}He, and the third proton which has to be in a p or higher quantum state relative to the spectator ^{2}He; therefore, the use of three-body phase space is more appropriate than the use of four-body phase space.

Evidence for a $T=3/2$ (three-neutron) resonance [22,23] was also deduced from inclusive spectra from the pion-induced double-charge-exchange (DCX) reaction ^{3}He$(\pi^-,\pi^+)3n$. Spectra measured at incident pion energies $T_\pi=140$ MeV and 200 MeV revealed cross section enhancements at forward angles that were claimed to resemble a broad resonance centered at about 17.5–20 MeV and of 21–32 MeV width. This three-neutron resonance should be the isobaric analog of the three-proton resonance suggested in Ref. [20] but the large difference between the proposed excitation energies (10 MeV in the three-proton system versus 17.5–20 MeV for the three-neutron system) raises doubts regarding the validity of the claim that the ^{3}He$(\pi^-,\pi^+)3n$ reaction discovered a resonance in the $3n$ system.

The DCX reaction was thought to be well suited for such a study because the reaction mechanism must primarily involve two target nucleons, so that there can be no quasifree nucleon knockout process; however, new measurements [57] at $T_\pi=240$ MeV, in qualitative agreement with Refs. [22,23], were interpreted successfully without invoking a three-nucleon resonance. A model [58] developed for ^{4}He$(\pi^-,\pi^+)4p$, assuming two sequential single-charge exchanges, $(\pi^-p\rightarrow\pi^0n)$ followed by $(\pi^0p\rightarrow\pi^+n)$, reproduced the forward-angle data from the ^{3}He target very well.

In this paper we have shown that at intermediate energy (200 MeV) the ^{3}He(p,n) reaction proceeds primarily by a QF scattering process. We suggest that the broad peak [20] in the neutron spectrum from ^{3}He(p,n) measured at 20° and $T_p=48.8$ MeV does not result from a $3p$ resonance but rather from a significant contribution of the quasifree charge-exchange process. The momentum transfer at this angle and energy is ≈0.5 fm^{-1} which is roughly the same momentum transfer as at 10° and 200 MeV in our experiment; therefore, we renormalized our double-differential cross sections by the ratio $R=0.53$ of elementary NN cross sections at 200 and 48.8 MeV extracted from SAID [27] and found that the spectrum from Ref. [20] agrees very well with our renormalized spectrum (Fig. 13). Thus the spectrum measured at the low incident energy is consistent with a quasifree process and should not be used as evidence for a $T=3/2$ resonance in mass 3.

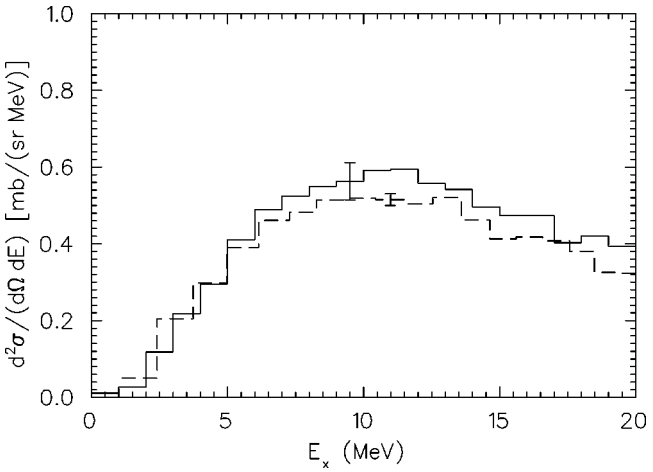

FIG. 13. Excitation energy spectra for ^{3}He(p,n) at $\theta_{\rm lab}=20°$ and $T_p=48.8$ MeV (solid line) and at $\theta_{\rm lab}=10°$ and $T_p\approx200$ MeV (dashed line). The latter was renormalized by the ratio of free NN cross sections at these two energies.

Very recent theoretical work [59] on the $T=3/2$ system, $3n$ and $3p$, suggests the lowest $3p$ resonance to be a state of $J^\pi=3/2^+$ at 15 MeV excitation and of width $\Gamma=14$ MeV. The dominant terms in the wave function of this $3/2^+$ state are, in familiar notation, the $[(l_1l_2)L,S]=[(1\ \ 1)\ 1,\ 3/2]$ and $[(1\ 1)\ 2,\ 3/2]$ components. The ^{3}He(p,n) reaction can excite these components from the dominant g.s. configuration $[(0\ 0)\ 0,\ 1/2]$ only by a two-step process or from one of the small components in the g.s. by a simple (p,n) charge exchange. In either case, the cross sections are expected to be small. Thus, the fact that we do not observe a peak in our spectra near 14 MeV cannot be taken as evidence against the existence of the theoretically predicted $3/2^+$ state.

VI. CONCLUSION

The neutron spectra $d^2\sigma/(d\Omega\ dE_x)$ from the inclusive ^{3}He$(\vec{\rm p},n)$ reaction at 200 MeV were found to be distinctly different from those for ^{4}He$(\vec{\rm p},n)p^3$He; however, the ratio of double-differential cross sections for ^{4}He and ^{3}He, integrated over E_x, was observed to be close to 2, independent of the scattering angle, as expected for a quasifree process. Whereas the ^{4}He$(\vec{\rm p},n)p^3$He reaction revealed a strong resonant FSI in the $p+^3$He two-particle system owing to the well-known $L=1$ resonances, there was no evidence for a resonant FSI in the $p+^2$He system. For ^{3}He, the experimental analyzing powers averaged over E_x agree well with the results from free NN scattering, supporting the notion of a predominantly quasifree scattering mechanism. For ^{4}He, the A_y are generally larger than the free scattering values especially at a few forward angles. A strong suppression of the far forward-angle cross sections compared with the free NN

values is observed for both targets and is attributed to Pauli blocking of the $\Delta L=0$ transition.

At most angles, calculations with the quasifree scattering code THREEDEE were successful in fitting the qualitative features of the data both for ^{3}He and ^{4}He. In order to describe the strong cross section enhancement for ^{4}He(p,n) at low E_x in ^{4}Li (small relative p^3He energies) we modified THREEDEE to include a sequential-coordinate formalism. These calculations fitted the yields near threshold as well as the continuum at higher E_x quite well. For a good fit to the data it was essential that we used an optical potential that exhibits a strong $L=1$ potential resonance in the $p+^3$He system.

Neither the THREEDEE calculations nor the data show such resonance enhancements for ^{3}He(p,n). The positions and widths of the QF peaks are reproduced well by the THREEDEE calculations using a potential for the $p+2p$ system that does not exhibit a potential resonance. Thus our data and analysis do not support the evidence for the $T=3/2$ (three-proton) resonance deduced from ^{3}He(p,n) spectra at incident energies below 50 MeV; however, we cannot exclude the existence of states that would be excited primarily by two-step or more complex processes as the cross sections may be too small to be observable.

ACKNOWLEDGMENTS

The authors wish to thank the staff at IUCF for technical assistance. This work was supported in part by the U.S. Department of Energy and the National Science Foundation.

[1] J. Rapaport and E. Sugarbaker, Annu. Rev. Nucl. Part. Sci. **44**, 109 (1994).
[2] L. Wang *et al.*, Phys. Rev. C **50**, 2438 (1994).
[3] D. L. Prout *et al.*, Phys. Rev. C **52**, 228 (1995).
[4] J. Wambach, Phys. Rev. C **46**, 807 (1992).
[5] R. A. Brandenburg, Y. E. Kim, and A. Tubis, Phys. Rev. C **12**, 1368 (1975).
[6] I. R. Afnan, Phys. Rev. C **16**, 823 (1977).
[7] B. Blankleider and R. M. Woloshyn, Phys. Rev. C **29**, 538 (1984).
[8] J. L. Friar, B. F. Gibson, G. L. Payne, and C. R. Chen, Phys. Rev. C **34**, 1463 (1986).
[9] J. Carlson, Nucl. Phys. **A522**, 185c (1991).
[10] D. L. Prout *et al.*, in ''Proceedings of the XV International Conference on Few-Body Problems in Physics,'' 1997, Groningen, The Netherlands, edited by L. P. Kok, J. C. S. Bacelar, and A. E. L. Dieperink (unpublished), p. 270; D. L. Prout, M. Palarczyk, and B. Anderson, IUCF Experiments E385 and E387 (unpublished).
[11] A. Rahav *et al.*, Phys. Lett. B **275**, 259 (1992); Phys. Rev. C **46**, 1167 (1992).
[12] E. J. Brash *et al.*, Phys. Rev. C **47**, 2064 (1993).
[13] M. Miller *et al.*, Phys. Rev. Lett. **74**, 502 (1995).
[14] R. G. Milner *et al.*, Phys. Lett. B **379**, 67 (1996).
[15] R.-W. Schulze and P. U. Sauer, Phys. Rev. C **48**, 38 (1993).
[16] J. Carlson and R. Schiavilla, Phys. Rev. Lett. **68**, 3682 (1992).
[17] V. R. Pandharipande *et al.*, Phys. Rev. C **49**, 789 (1994).
[18] C. M. Edwards, Ph.D. thesis, University of Minnesota, 1996 (unpublished).
[19] C. M. Edwards *et al.*, Phys. Lett. B **368**, 39 (1996); **380**, 493(E) (1996).
[20] L. E. Williams *et al.*, Phys. Rev. Lett. **23**, 1181 (1969).
[21] A. D. Bacher *et al.*, Phys. Lett. **29B**, 573 (1969) and references therein.
[22] J. Sperinde *et al.* Phys. Lett. **32B**, 185 (1970); J. Sperinde, D. Fredrickson, and V. Perez-Mendez, Nucl. Phys. **B78**, 345 (1974).
[23] A. Stetz *et al.*, Nucl. Phys. **A457**, 669 (1986).
[24] J. Arvieux, Nucl. Phys. **A221**, 253 (1974).
[25] D. R. Tilley, H. R. Weller, and G. M. Hale, Nucl. Phys. **A541**, 1 (1992).
[26] N. S. Chant and P. G. Roos, Phys. Rev. C **15**, 57 (1977); N. S. Chant, P. Kitching, P. G. Roos, and L. Antonuk, Phys. Rev. Lett. **43**, 495 (1979); N. S. Chant and P. G. Roos, Phys. Rev. C **27**, 1060 (1983); N. S. Chant, computer code THREEDEE, University of Maryland, 1992 (unpublished).
[27] R. A. Arndt and L. D. Roper, Scattering Analysis Interactive Dial-in Program SAID, Virginia Polytechnic Institute and State University (unpublished). Phase shift sets SM95 (for free *NN* observables) and SM89 (for free *NN* phase shifts used in THREEDEE).
[28] C. D. Goodman *et al.*, IEEE Trans. Nucl. Sci. **NS-26**, 2248 (1979).
[29] J. N. Knudson *et al.*, Phys. Rev. C **22**, 1826 (1980).
[30] G. L. Moake *et al.*, Phys. Rev. Lett. **43**, 910 (1979).
[31] X. Yang *et al.*, Phys. Rev. C **48**, 1158 (1993).
[32] J. Rapaport *et al.*, Phys. Rev. C **24**, 335 (1981).
[33] T. N. Taddeucci *et al.*, Nucl. Phys. **A469**, 125 (1987).
[34] C. Gaarde *et al.*, Nucl. Phys. **A369**, 258 (1981).
[35] F. James, ''FOWL— A General Monte-Carlo Phase Space Program,'' CERN Library, 1977).
[36] R. J. N. Phillips, Nucl. Phys. **53**, 650 (1964).
[37] G. F. Bertsch and O. Scholten, Phys. Rev. C **25**, 804 (1982).
[38] K. M. Watson, Phys. Rev. **88**, 1163 (1952).
[39] J. Gillespie, in *Final-State Interactions*, Holden-Day Advanced Physics Monographs, edited by K. M. Watson (Holden-Day, San Francisco, 1964).
[40] R. D. Lawson, *Theory of the Nuclear Shell Model* (Clarendon Press, Oxford, 1980).
[41] D. F. Jackson and T. Berggren, Nucl. Phys. **62**, 353 (1965).
[42] M. K. Jones *et al.*, Phys. Rev. C **46**, 52 (1992).
[43] C. M. Edwards *et al.*, in *Polarization Phenomena in Nuclear Physics*, edited by E. J. Stephenson and S. E. Vigdor, AIP Conf. Proc. No. 339 (AIP, New York, 1995), p. 438.
[44] W. T. H. van Oers *et al.*, Phys. Rev. C **25**, 390 (1982).
[45] R. M. DeVries, J. L. Perrenoud, and I. Slaus, Nucl. Phys. **A188**, 449 (1972).
[46] J. S. Wesick, Ph.D. thesis, University of Maryland, 1984; J. S. Wesick *et al.*, Phys. Rev. C **32**, 1474 (1985).
[47] P. Schwandt (private communication).
[48] B. S. Podmore and H. S. Sherif, in *Few Body Problems in Nuclear and Particle Physics*, edited by R. J. Slobodrian, B.

Cujec, and K. Ramavartaram (Laval University Press, Quebec, Canada, 1975), p. 517.
[49] Y. Horikawa, F. Lenz, and N. C. Mukhopadhyay, Phys. Rev. C **22**, 1680 (1980).
[50] T. K. Lim, Phys. Lett. B **43**, 349 (1973); **44**, 341 (1973).
[51] R. Schiavilla, V. R. Pandharipande, and R. B. Wiringa, Nucl. Phys. **A449**, 219 (1986).
[52] P. Roos (unpublished).
[53] E. F. Redish, G. J. Stephenson, Jr., and G. M. Lerner, Phys. Rev. C **2**, 1665 (1970).
[54] T. Kaneko, H. Kanada, and Y. C. Tang, Few-Body Syst. **18**, 1 (1995); Y. C. Tang (private communication).
[55] A. Okihana *et al.*, RCNP, Osaka University, Annual Report, 1990, p. 43.
[56] B. D. Anderson *et al.*, Phys. Rev. C **54**, 1531 (1996).
[57] J. L. Matthews, in *Mesons and Nuclei at Intermediate Energies*, Proceedings of the International Conference on Mesons and Nuclei at Intermediate Energies, Dubna, Russia, 1994, edited by M. Kh. Khnakhasayev and Zh. B, Kurmanov (World Scientific, Singapore, 1995), p. 495.
[58] E. R. Kinney *et al.*, Phys. Rev. Lett. **57**, 3152 (1986).
[59] A. Csoto, H. Oberhummer, and R. Pichler, Phys. Rev. C **53**, 1589 (1996).